Advanced Research Center for Beam Science – Electron Microscopy and Crystal Chemistry –

http://eels.kuicr.kyoto-u.ac.jp:8080/Root/English

Prof
KURATA, Hiroki
(D Sc)

Assist Prof
NEMOTO, Takashi
(D Sc)

Assist Prof
HARUTA, Mitsutaka
(D Sc)

Program-Specific Res*
OGAWA, Tetsuya
(D Sc)

Program-Specific Res*
KIYOMURA, Tsutomu

*Nanotechnology Platform

Res
MORIGUCHI, Sakumi
(D Sc)

Assist Techn Staff

HIRAIZUMI, Yuri

Students

FUJIYOSHI, Yoshifumi (D3)
YAMAGUCHI, Atsushi (D1)
MITSUTA, Itaru (M2)
TOMISAKI, Yuriko (M1)

Scope of Research

Crystallographic and electronic structures of materials and their transformations are studied through direct imaging of atoms or molecules by high-resolution electron spectromicroscopy which realizes energy-filtered imaging and electron energy-loss spectroscopy as well as high resolution imaging. By combining this with scanning probe microscopy, the following subjects are urging: direct structure analysis, electron crystallographic analysis, epitaxial growth of molecules, structure formation in solutions, and fabrication of low-dimensional functional assemblies.

KEYWORDS

Surface Plasmon
EELS
Dispersion Curve
STEM
Transition-Metal Oxide

Selected Publications

Minari, T.; Nemoto, T.; Isoda, S., Temperature and Electric-field Dependence of the Mobility of a Single-grain Pentacene Field-effect Transistor, *J. Appl. Phys*., **99,** [034506-1]-[034506-5] (2006).

Haruta, M.; Kurata, H.; Komatsu, H.; Shimakawa, Y.; Isoda, S., Site-resolved Oxygen K-edge ELNES of Layered Double Perovskite La_2CuSnO_6, *Physical Review B*, **80,** [165123-1]-[165123-6] (2009).

Haruta, M.; Kurata, H., Direct Observation of Crystal Defects in an Organic Molecular Crystals of Copper Hexachlorophthalocyanine by STEM-EELS, *Sci. Rep*., **2,** [252-1]-[252-4] (2012).

Aso, R.; Kan, D.; Shimakawa, Y.; Kurata, H., Atomic Level Observation of Octahedral Distortions at the Perovskite Oxide Heterointerface, *Sci. Rep*., **3,** [2214-1]-[2214-6] (2013).

Saito, H.; Namura, K.; Suzuki, M.; Kurata, H., Dispersion Relations for Coupled Surface Plasmon-polariton Modes Excited in Multilayer Structures, *Microscopy*, **63,** 85-93 (2014).

Dispersion Relations for Coupled Surface Plasmon-polariton Modes Excited in Multilayer Structures

The coupled surface plasmon-polariton (SPP) modes excited in an Al/SiO_2/Al multilayer structure were analyzed using angle-resolved electron energy-loss spectroscopy (AREELS) with a relativistic electron probe. Three dispersion curves for coupled antisymmetric short range (AC-SR), symmetric short range (SC-SR) and antisymmetric long rang (AC-LR) modes were observed, but the symmetric long range (SC-LR) mode could not be detected because of its low excitation probability. The obtained dispersion curves agreed well with the calculated curves when an aluminum oxide layer was present on the surfaces, which indicates that the dispersion relations are very sensitive to multilayer surface conditions. In the multilayer structures, the dispersion relation for the coupled SPP modes was found to be sensitive to the thickness of each film, which could be interpreted qualitatively by the electron energy-loss probability calculated for thin aluminum (Al) films and narrow Al gaps using Kröger's formula. It was demonstrated that significant differences in the excitation probability for SPPs could be observed depending on the coupling modes.

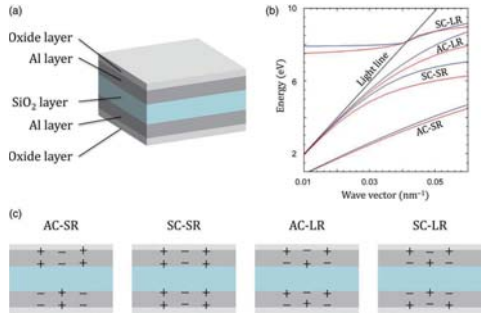

Figure 1. (a) Model of the multilayer structure for the dispersion calculation. (b) Examples of dispersion calculations. The red curves were calculated for the multilayer structure of AlO_x(3 nm)/Al(13 nm)/SiO_2(23 nm)/Al(13 nm)/AlO_x(3 nm). The blue curves were calculated for the multilayer without aluminum oxide layers of Al(16 nm)/SiO_2(23 nm)/Al(16 nm). (c) Schematic diagram of the charge distribution for each of the coupled SPP modes.

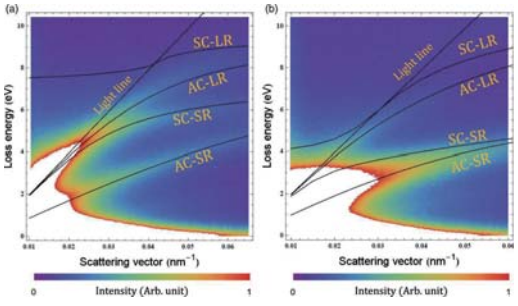

Figure 2. *E*−*q* maps obtained from (a) sample A and (b) sample B. The black curves are the dispersion curves for the coupled SPP modes calculated. The assumed structures of multilayer are AlO_x(3 nm)/Al(13 nm)/SiO_2(23 nm)/Al(13 nm)/AlO_x(3 nm) for (a) sample A and AlO_x(3 nm)/Al(7 nm)/SiO_2(61 nm)/Al(7 nm)/AlO_x(3 nm) for (b) sample B.

Control of Structural Distortions in Transition-metal Oxide Films through Oxygen Displacement at the Heterointerface

Structural distortions in the oxygen octahedral network in transition-metal oxides play crucial roles in yielding a broad spectrum of functional properties, and precise control of such distortions is a key for developing future oxide-based electronics. Here, it is shown that the displacement of apical oxygen atom shared between the octahedra at the heterointerface is a determining parameter for these distortions and consequently for control of structural and electronic phases of a strained oxide film. The present analysis by complementary annular dark- (HAADF) and bright-field (ABF) imaging in aberration-corrected scanning transmission electron microscopy (STEM) reveals that structural phase differences in strained monoclinic and tetragonal $SrRuO_3$ (SRO) films grown on $GdScO_3$ (GSO) substrates result from relaxation of the octahedral tilt, associated with changes in the in-plane displacement of the apical oxygen atom at the heterointerface. It is further demonstrated that octahedral distortions and magnetrotransport properties of the $SrRuO_3$ films can be controlled by interface engineering of the oxygen displacement. This provides a further degree of freedom for manipulating structural and electronic properties in strained films, allowing the design of novel oxide-based heterostructures.

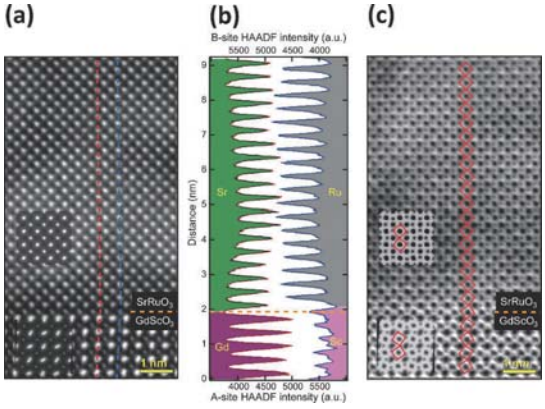

Figure 3. High-resolution cross-sectional HAADF- and ABF-STEM images of SRO/GSO heterostructure and element characterization. (a) High-resolution HAADF image of the 23 nm-thick tetragonal SRO thin film grown on the GSO substrate taken along the [001] ortho direction. Simulated HAADF images of bulk SRO and GSO with orthorhombic structures are also inserted in the image. (b) HAADF intensity profiles of A-site (left side) and B-site (right side) cations across the heterointerface. The data were collected along the red and blue dashed lines for A- and B-site cationic rows in (a), respectively. In the profiles, Sr (Z = 38), Gd (Z = 64), Ru (Z = 44), and Sc (Z = 21) atomic columns are colored in green, purple, gray, and pink, respectively. The interface position is denoted by the orange dashed line. (c) ABF image taken from the same region as the HAADF image (a). In the image, oxygen atoms are clearly visible as dark contrast, revealing the projected shape of each oxygen octahedron and the octahedral connection across the interface as indicated with red solid rectangles. The simulated ABF images of bulk SRO and GSO are also included.